Lasers in Surgery and Medicine 38:155–162 (2006)

Improvement of Port Wine Stain Laser Therapy by Skin Preheating Prior to Cryogen Spray Cooling: A Numerical Simulation

Wangcun Jia, PhD,[1]* Guillermo Aguilar, PhD,[1,2] Wim Verkruysse, PhD,[1] Walfre Franco, PhD,[1,2] and J. Stuart Nelson, MD, PhD[1]
[1]*Beckman Laser Institute, University of California, Irvine, California 92612*
[2]*Department of Mechanical Engineering, University of California, Riverside, California 92521*

Background and Objectives: Although cryogen spray cooling (CSC) in conjunction with laser therapy has become the clinical standard for treatment of port wine stain (PWS) birthmarks, the current approach does not produce complete lesion blanching in the vast majority of patients. The objectives of this study are to: (1) experimentally determine the dynamic CSC heat flux when a skin phantom is preheated, and (2) numerically study the feasibility of using skin preheating prior to CSC to improve PWS laser therapeutic outcome.
Study Design/Materials and Methods: A fast-response thin-foil thermocouple was used to measure the surface temperature and thus heat flux of an epoxy skin phantom during CSC. Using the heat flux as a boundary condition, PWS laser therapy was simulated with finite element heat diffusion and Monte Carlo light distribution models. Epidermal and PWS blood vessel thermal damage were calculated with an Arrhenius-type kinetic model.
Results: Experimental results show that the skin phantom surface can be cooled to a similar minimum temperature regardless of the initial temperature. Numerical simulation indicates that upon laser irradiation, the epidermal temperature increase is virtually unaffected by preheating, while higher PWS blood vessel temperatures can be achieved. Based on the damage criterion we assumed, the depth and maximum diameter of PWS vessels that can be destroyed irreversibly with skin preheating are greater than those without.
Conclusions: Skin preheating prior to CSC can maintain epidermal cooling while increasing PWS blood vessel temperature before laser irradiation. Numerical models have been developed to show that patients may benefit from the skin preheating approach, depending on PWS vessel diameter and depth. Lasers Surg. Med. 38:155–162, 2006. © 2006 Wiley-Liss, Inc.

Key words: cryogen spray cooling; skin preheating; laser dermatologic surgery; vascular malformation; thin-foil thermocouple; Duhamel theorem; Monte Carlo

INTRODUCTION

The objective of port wine stain (PWS) laser treatment is to maximize thermal damage to the targeted blood vessels while preventing injury to the normal overlying epidermis. Unfortunately, for many lesions, the threshold laser dosage for epidermal damage may be lower than that required for permanent PWS blanching. An important approach to the aforementioned problem is to selectively cool the most superficial layers of the skin with cryogen spray cooling (CSC), which has led to improved therapeutic outcome of PWS and other vascular lesions [1–7]. However, the current approach to PWS laser surgery does not produce complete lesion blanching in the vast majority of patients [8–10]. One reason for treatment failure is that heat generation within large PWS vessels is confined to the upper portion thereof because the light penetration depth in blood is too short at the wavelengths (585–595 nm) currently used for therapy [11]. Skin preheating prior to CSC has the potential to permit lowering the light dosage required for irreversible vascular photocoagulation of large diameter PWS blood vessels.

We hypothesize that, by preheating the skin prior to CSC, comparable epidermal and higher PWS blood vessel temperatures will be obtained than when using CSC alone. Skin temperature can be increased by 10–15°C higher than normal body temperature by preheating using a hot air jet, infrared irradiation, etc. Since CSC heat flux increases with initial skin temperature [12], the epidermis can be cooled more effectively while higher temperatures within the PWS vessels induced during the preheating period can be preserved. Because the PWS blood vessel temperature is raised from baseline while keeping the epidermis selectively cooled, two advantageous effects would be attained. First, preheating would not have any effect on the incident irradiance allowed. Second, the temperature increase required to photocoagulate preheated blood vessels would be less, which means that lower light dosage is required.

Contract grant sponsor: National Institutes of Health; Contract grant numbers: GM 62177, AR 48458, AR 47551, HD42057; Contract grant sponsor: Beckman Laser Institute Endowment.
*Correspondence to: Wangcun Jia, PhD, Beckman Laser Institute, 1002 Health Sciences Road East, Irvine 92612-1475, CA. E-mail: wjia@uci.edu.
Accepted 15 September 2005
Published online 23 February 2006 in Wiley InterScience (www.interscience.wiley.com).
DOI 10.1002/lsm.20255

A previous theoretical study has shown that skin preheating with a near-infrared laser in conjunction with surface cooling could increase the depth of selective damage of blood vessels [13]. In that study, cooling of the skin was simulated by applying a layer of either water at a temperature of 0°C or liquid nitrogen at a temperature of −196°C, which are not used clinically. The skin was simulated as four layers, and vessels were simulated rather unrealistically as a layer of homogeneous distribution of blood.

In the present study, we first determined experimentally the dynamic CSC heat flux ($q''(t)$) extracted from an epoxy skin phantom using a fast-response thin-foil thermocouple when the skin phantom was preheated to different initial temperatures (T_0). We then developed numerical models of heat diffusion, light distribution, and tissue damage with a more realistic multiple cylindrical blood vessel model of PWS skin. The measured $q''(t)$ is used as thermal boundary condition in the heat diffusion model. Finally, using these numerical models, we studied the use of skin preheating prior to CSC to improve PWS laser therapeutic outcome. The rationale behind the study is that: (1) CSC would effectively maintain the temperature of preheated epidermis below the threshold for thermal damage, and (2) the light dosage required to photocoagulate preheated blood vessels would be less.

MATERIALS AND METHODS

Cryogen Delivery and Nozzle

The cryogen utilized was 1,1,1,2 tetrafluoroethane, also known as R-134a, with saturation temperature $T_{sat} \approx -26.2$°C at atmospheric pressure. Cryogen was kept in a container at its saturation pressure (660 kPa at 25°C) and delivered through a high-pressure hose to an electronically controlled fuel injector attached to a straight-tube nozzle. The nozzle was made of stainless steel with an inner diameter (d_N) and length (l_N) of 0.7 and 63.6 mm, respectively. The nozzle was soldered to a custom-made copper coupling which fit tightly around the fuel injector. The nozzle d_N and spurt duration (50 milliseconds) were similar to those in current clinical use for PWS laser surgery.

Temperature Measurement Sensor and Skin Phantom

An essential boundary condition in the simulation of CSC-assisted PWS laser therapy is the dynamic CSC heat flux [$q''(t)$]. Different thermal sensors have been developed to determine $q''(t)$ [14–16]. These sensors have large bead diameters (50–300 μm) as compared to the thickness of human epidermis (50–100 μm) and relatively long response times. In this study, a thin-foil K type thermocouple (CO2-K, Omega Engineering, Stamford, CT) was utilized to determine $q''(t)$ when a skin phantom was preheated. Although the width and length of its measurement junction are around 0.5 mm, the thin-foil sensor has a thickness of only 13 μm, resulting in a higher vertical temperature resolution than conventional wire sensors. This feature makes the thin-foil sensor suitable for measuring surface temperature during CSC because the vertical temperature gradient in either skin phantom or human skin is much higher than that in the lateral direction [17]. The estimated response time is around 2 millisecond and measurement uncertainty associated with K-type thermocouples is about ±0.2°C after calibration.

The skin phantom was composed of an epoxy resin (EP30-3, Master Bond, Inc., Hackensack, NJ), which has a thermal conductivity (λ) of 0.14 W/(m·K), specific heat capacity (c) of 1,631 J/(kg·K), and density (ρ) of 1,019 kg/m^3 [18]. Therefore, the epoxy skin phantom has a thermal diffusivity of 0.84×10^{-7} m^2/second, which is within 25% of that for human skin, 1.1×10^{-7} m^2/second [19]. This skin phantom was placed underneath a hot air jet and cryogen nozzle, as shown in Figure 1. The hot air jet was used to heat the phantom surface to the desired temperature before application of a cryogen spurt.

To minimize the thermal contact resistance between the thin-foil sensor and the epoxy skin phantom, the following procedures were followed to bond the sensor. The top surface of a flat Teflon® block was covered with double sided tape and the sensor was adhered onto the tape. A Teflon® enclosure was then placed around the sensor to form a mold. Thereafter, a degassed liquid mixture of epoxy and curing agent was poured into the mold in a vacuum chamber to avoid trapping air bubbles. After the epoxy was cured, the mold and tape were removed carefully with the aid of isopropyl alcohol.

We assume that the thermal contact resistance between the sensor and the epoxy phantom is small enough so that the temperature measured by the sensor is that of the surface. Experiments and simulations were performed to validate this assumption. In the experiments, we obtained temperature measurements when the sensor was directly

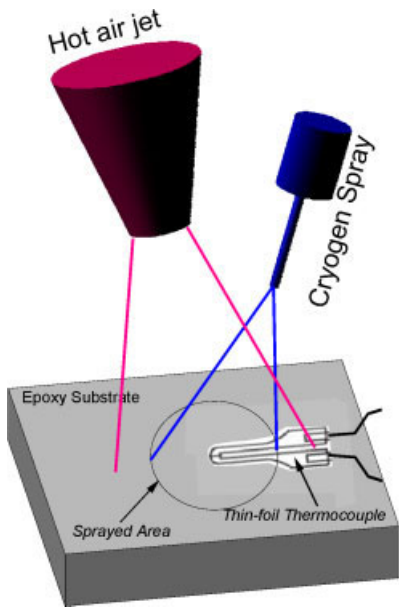

Fig. 1. Schematic of skin preheating and CSC.

exposed to CSC and when the sensor was covered with a layer of Scotch® tape of known thickness (50 or 78 μm). The Scotch® tape has a λ of 0.22 W/(m · K), c of 1,400 J/(kg · K), and ρ of 1,280 kg/m^3, which are similar to those of epoxy [17]. The nozzle-to-surface distance (z) was fixed at 20 mm, and the spurt duration (Δt) at 50 millisecond. In the simulation, the two-dimensional transient heat conduction equation was solved with a finite-element method software (FEMLAB®) to predict the temperature variation below the tape. The simulation geometry has a tape layer and an epoxy block with a size of 6×6 mm. Thermal insulation was assumed at both sides and at the bottom of the geometry. The measured temperature when the sensor was directly exposed to CSC was used as the boundary condition at the top of the tape layer. Both the measured and simulated temperatures below the 50 and 78 μm thick tapes, as well as the temperature measured without tape are shown in Figure 2. Reasonably good agreement between measured and predicted temperature variations at two depths is achieved, which proves the measured temperature at the surface is very close to that of the phantom surface during CSC.

Once the surface temperature history, $T_s(t)$, is obtained with the thin-foil thermocouple before, during and after CSC, the $q''(t)$ at the surface can then be conveniently obtained using the one-dimensional, semi-infinite medium solution for a step change in surface temperature and applying Duhamel's superposition integral [17,20] to give:

$$q''(t) = \sqrt{\frac{\rho c \kappa}{\pi}} \int_0^{T_s(t)} \frac{1}{\sqrt{t-\tau}} \mathrm{d}T_s(\tau) = \sqrt{\frac{\rho c \kappa}{\pi}} \int_0^{t} \frac{1}{\sqrt{t-\tau}} \frac{\mathrm{d}T_s(\tau)}{\mathrm{d}\tau} \mathrm{d}\tau \quad (1)$$

This method to determine $q''(t)$ is more accurate and convenient than an inverse heat-conduction algorithm, which uses temperature data measured at a subsurface location with conventional wire thermocouples.

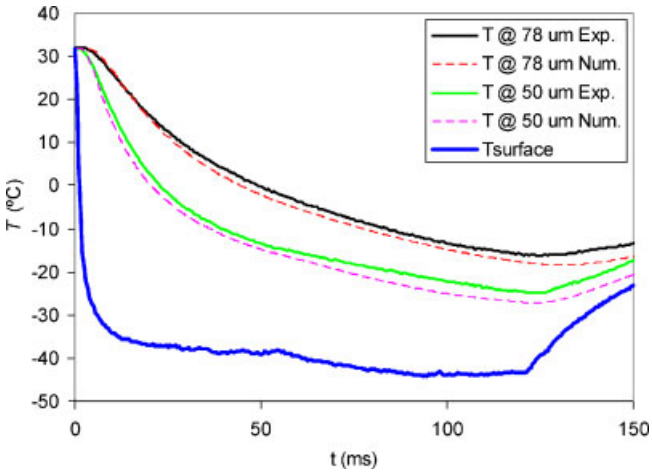

Fig. 2. Measured temperatures at the surface and beneath 50- and 78-μm-thick tapes. The dashed lines show simulated temperatures at the same depths using the measured temperatures at the surface without tape as boundary condition.

Numerical Models

The numerical models have three main components: 1) a Monte Carlo (MC) light distribution model, 2) a finite-element solution to the heat-conduction equation, and 3) an Arrhenius rate process integral to calculate thermal damage. The MC model simulates light transport in human skin to produce energy deposition per unit time per unit skin volume during pulsed laser exposure, $S(r,z,t)$, where r and z are lateral and depth dimensions, respectively. The thermal diffusion model simulates heat transfer in human skin during preheating, CSC, pulsed laser exposure, and a thermal relaxation phase to compute the time-dependent temperature distribution in human skin. The Arrhenius rate process integral calculates tissue denaturation ratio to predict epidermal thermal damage and blood photocoagulation. Each of these models is described in detail below.

The MC model used in this study was developed by Keijzer and coworkers [21–23], and the details will not be repeated here. The skin is modeled by two infinitely wide layers representing the epidermis and dermis of 60 and 940∼1940 μm thicknesses, respectively (see Fig. 3). Vessels with six different diameters, ranging from 50–130 μm, are placed in the dermis 200–900 μm below the skin surface. The distribution of vessels shown in Figure 3 is extended infinitely to the left and right. We simulate an incident laser beam of infinite diameter, which is a good approximation for the spot size in current clinical use [22,24]. The wavelength of 585 nm is commonly used for PWS laser treatment. The optical properties for each skin component [25] are listed in Table 1. In our model, melanin is homogeneously distributed in the epidermis using volume fractions (MVF) of 5, 10, and 15%, which approximately correspond to lightly, moderately, and darkly pigmented skin patients, respectively. Blood is represented by the optical properties of hemoglobin. We assume the hematocrit is 40% and the hemoglobin is distributed homogeneously in the vessel.

The two-dimensional transient heat-conduction equation:

$$\kappa \nabla^2 T(r,z,t) + S(r,z,t) = \rho c \frac{dT(r,z,t)}{dt} \quad (2)$$

is solved with a finite element method (FEM) using a commercial package, FEMLAB®. The thermal properties of skin [19,26] used in this model are listed in Table 2. The heat-source term, S, is present only during pulsed laser exposure. A constant initial temperature of 35°C is used for the entire tissue volume before preheating. Adiabatic boundary conditions are applied at $z = \infty$ and $r = \pm\infty$. The thermal boundary condition at the skin surface ($z = 0$) is as follows: a heat transfer coefficient of 200 W/(m^2 · K) [27] and an ambient temperature of 60°C during hot air jet preheating; CSC heat flux determined in the proposed experiment during an effective CSC cooling period (spurt duration plus cryogen residence time [12]); a natural convection heat transfer coefficient of 10 W/(m^2 · K); and an

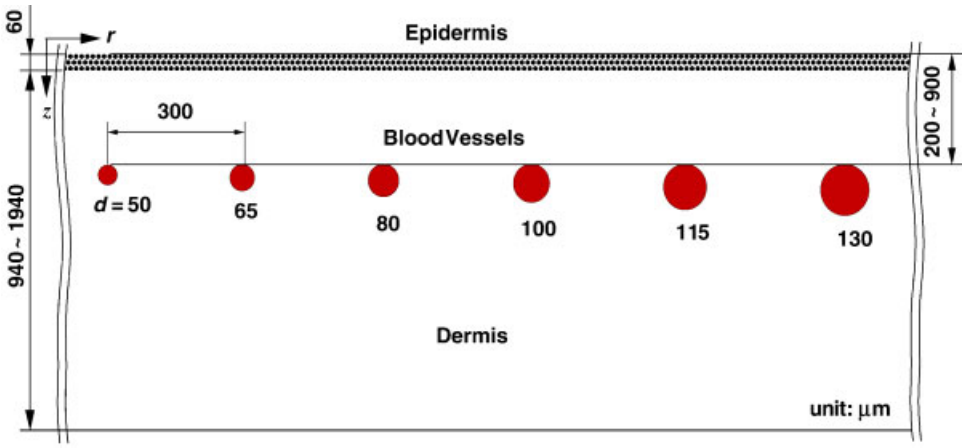

Fig. 3. Dimensions of model human skin with discrete PWS blood vessels.

ambient temperature of 25°C after laser irradiation. The period of preheating is 40 seconds, the cooling period of CSC is 60–100 milliseconds depending on vessel depth, and the laser pulse duration is 1.5 millisecond.

The Arrhenius rate process integral is used to quantify epidermis and PWS blood vessel thermal damages:

$$\Omega(r,z,\tau) = \ln\left[\frac{C_n(r,z,0)}{C_n(r,z,\tau)}\right] = A\int_0^\tau \left\{\exp\left[-\frac{\Delta E}{RT(r,z,t)}\right]dt\right\} \quad (3)$$

where C_n is the remaining concentration of native state tissue at exposure time t and R is the universal gas constant (8.314 J/(mole·K)). We use the values $A = 1.8\times10^{51}$ /second and $\Delta E = 327{,}000$ J/mole for bulk skin [28], and $A = 7.6\times10^{66}$ /second and $\Delta E = 455{,}000$ J/mol for blood [29]. Calculations of Ω are maintained for a period of time after laser irradiation until thermal damage accumulation has ceased.

RESULTS

In this section, experimental results on the heat transfer dynamics during CSC at different initial substrate temperatures (T_0) and numerical results on the temperature distributions and thermal damages in model PWS skin are presented.

Heat Transfer Dynamics During CSC at Different T_0

Figure 4a shows measured surface temperatures (T_s) as a function of time at three different T_0 of 35, 50, and 80°C. For all measurements, the nozzle-to-surface distance (z) was 20 mm, and the spurt duration (Δt) was 50 milliseconds. Initially, T_s values decreased sharply during a short period of time (12 millisecond, indicated by line I). This time is only half of that obtained with a wire thermocouple [15,26,30], illustrating that the thin-foil thermocouple resolves fast temperature changes at the surface better than sensors previously used [14–16]. This capability is critical to understand the dynamics of the short cryogen spurts (5–100 milliseconds), which are in current clinical use.

After the initial fast drop, T_s is kept below T_{sat} (−26.2°C) of R134a, as indicated by the horizontal line in Figure 4a, during a specific period of time (between lines I and II), which is even longer than the spurt duration. Such low surface temperatures are obtained because of the bombardment of cold cryogen droplets (−44.6°C, [31]) during the cryogen spurt and evaporation of residual cryogen at the cryogen–air interface after spurt termination. It should be realized that freezing of water in human skin might occur during this period. The fast increase of T_s, indicated by line II, suggests complete evaporation of residual cryogen. Although the differences between T_0 are as much as 45°C, the differences between minimum T_s are very small. When T_0 is 80°C, minimum T_s is −40°C, and −42°C when T_0 is 35°C. These findings are favorable for PWS laser surgery because the epidermal temperature reduction with CSC is not significantly affected by T_0.

Figure 4b shows the heat flux calculated with Equation 1. For each T_0, $q''(t)$ increased rapidly to a maximum value (q''_{max}) and then dropped gradually. Although $q''(t)$ curves are qualitatively similar to each other, q''_{max} increases with T_0. The q''_{max} for $T_0 = 80$°C is 47% higher than for

TABLE 1. Optical Properties of Various Skin Components Used in the Monte Carlo Model

Skin component	μ_a (1/cm)	μ_s (1/cm)	g
Epidermis	20, 40, 60	470	0.79
Dermis	1.9	129	0.79
Blood	191	467	0.99

TABLE 2. Thermal Properties of Various Skin Components Used in the Heat Transfer Model

Skin component	κ (W/m·K)	ρ (kg/m^3)	c (J/kg·K)
Epidermis	0.34	1,120	3,200
Dermis	0.41	1,090	3,500
Blood	0.55	1,060	3,600

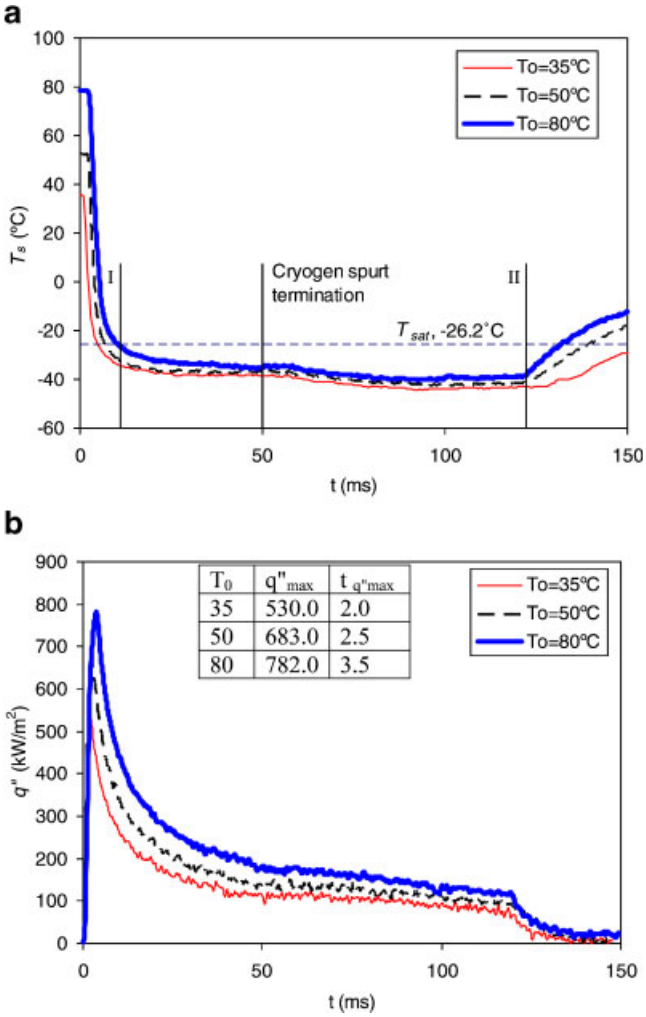

Fig. 4. Measured T_s (**a**) and calculated q'' (**b**) for $\Delta t =$ 50 milliseconds, $z = 20$ mm.

$T_0 = 35°C$. The effect of T_0 on the time needed to reach q''_{max} is not significant. Therefore, the total heat extracted from skin increased with T_0 within the clinically relevant cooling period. The interpolation of these $q''(t)$ curves is used as the thermal boundary condition for the numerical models since the model skin surface temperature is not exactly the same as T_0 in the experiments.

Simulated Temperature Distribution and Photocoagulation

In the preheating simulation, the model skin depth was 10 mm rather than the 1 or 2 mm used for laser heating due to deeper heat conduction during a long preheating period. After 40 seconds preheating with a 60°C hot air jet, the temperature within 1 mm of the model skin increased from 35°C to an average of 47°C. Epidermal temperature was 1–4°C higher than PWS blood vessel temperature depending on vessel depth. Tissue perfusion was neglected in the model because the blood perfusion time, that is, the reciprocal blood perfusion rate of dermis is normally in the range of 300~1,000 seconds depending on local skin temperature [32]. Apparently, skin preheating with a millisecond infrared laser pulse might be a better choice to minimize the influence of tissue perfusion. We also assumed no vasodilatation occurred as a result of preheating. This temperature distribution was used as the initial condition for the following simulation of CSC-assisted PWS laser therapy with preheating.

Figure 5 shows the temperature profiles across the center of an 100 μm diameter blood vessel as a function of depth at the end of the laser pulse with CSC only and with both preheating and CSC. The melanin volume fraction (MVF) is 15% (which represents a darker skin type patient) and blood vessels are 200 μm deep. The cooling period of CSC was 60 milliseconds without preheating, and 70 milliseconds with preheating prior to CSC. An extra 10 milliseconds of cooling of preheated skin is necessary to reach similar basal layer temperature reduction as that of normal skin. The laser fluence is 3.5 J/cm^2 and pulse duration is 1.5 milliseconds. It is clear that the temperature increase in the epidermis is virtually unaffected by preheating but higher core intravascular temperature is achieved with preheating prior to CSC. Note that the simulated blood temperature is higher than 100°C (the saturation temperature of water at an ambient pressure of 1 atm).

A color map of calculated Ω values for model skin using the Arrhenius rate process integral with CSC only is shown in Figure 6. The MVF, PWS vessel depth, CSC, and laser parameters were the same as above. The scale of Ω is set from zero to four to make the color map easy to read because $\Omega = 4$ already corresponds to a 98% decrease from the original total of undamaged tissue constituents. The damage threshold for tissue necrosis is selected as $\Omega = 1$ (a 63% decrease from the original total of undamaged tissue constituents). It can be seen that there is no sign of epidermal injury at the laser fluence of 3.5 J/cm^2. However, if the fluence is increased to 4 J/cm^2, epidermal injury is

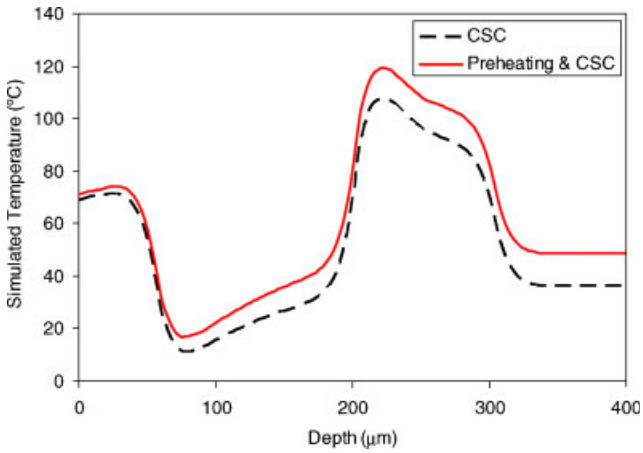

Fig. 5. Temperature profiles as a function of depth at the end of the laser pulse with CSC only (60 milliseconds) and with both preheating and CSC (70 milliseconds); MVF = 15%; PWS depth, 200 μm; laser, 3.5 J/cm^2, 1.5 milliseconds.

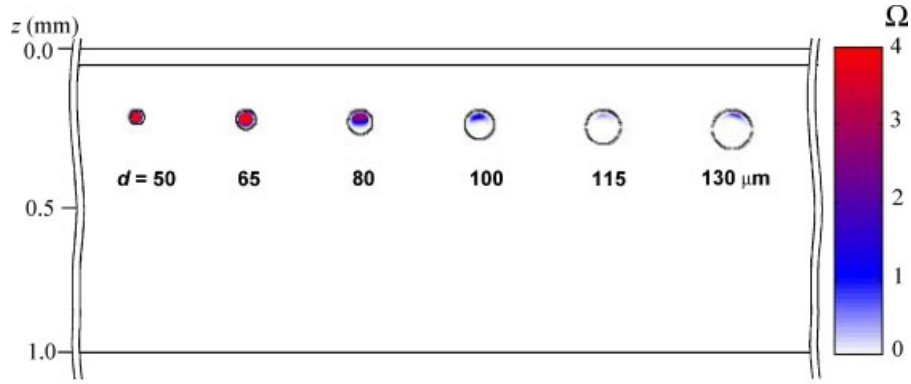

Fig. 6. Color map of calculated Ω values for the model skin without preheating; MVF = 15%; PWS depth, 200 μm; CSC, 60 milliseconds; laser, 3.5 J/cm^2, 1.5 milliseconds.

predicted by our simulation. As for blood vessel damage, we need to define a criterion to assess irreversible vessel damage. Previous theoretical models used a threshold average temperature of 70°C to predict vessel necrosis [13,33,34]. However, in vitro pulsed laser irradiation of whole blood showed that coagulation occurs at 80–90°C [35]. Instead of a threshold average temperature, the area ratio of coagulated blood to total blood in the vessel (r_c) is selected to assess irreversible vessel damage. If this ratio is higher than 64%, we assume the vessel is destroyed irreversibly [36].

Figure 7 shows r_c for vessels of different diameters with CSC only and with both preheating and CSC. The laser fluence was 3.5 J/cm^2 for both simulations, and no epidermal injury was predicted. It can be seen that r_c for large vessels (> 80 μm diameter) increased more than four times from an average of 15% for CSC only to 63% for both preheating and CSC. Based on the damage criterion we assumed, vessels with a diameter less than 65 μm will be destroyed irreversibly with CSC only but vessels with diameters of 100 μm will be destroyed irreversibly with both preheating and CSC. When PWS vessels are located 400 μm below the skin surface as shown in Figure 8, irreversible vessel damage cannot be caused with CSC only, even for the smallest vessels in the simulation. However, vessels with diameters less than 65 μm are destroyed irreversibly with skin preheating prior to CSC.

Figure 9 shows r_c for vessels of different diameters with CSC only and with both preheating and CSC when the MVF was 10%, which represents a moderately pigmented skin type patient. Depth of PWS vessels was 400 μm. The laser fluence was 4.5 J/cm^2 for both simulations. Above this fluence, epidermal injury was predicted by our simulation. It can be seen that r_c for large vessels (> 100 μm diameter) increased from an average of 53% for CSC only to 89% for both preheating and CSC. Based on the damage criterion we assumed, vessels of diameter less than 100 μm will be destroyed irreversibly with CSC only, but vessels with diameters of 130 μm will be destroyed irreversibly with both preheating and CSC.

Figure 10 shows r_c when the MVF is 5%, which represents a light skin type patient. Depth of PWS vessels was 900 μm. The laser fluence was 7 J/cm^2, the maximum allowed to avoid epidermal injuries for both simulations. It can be seen that r_c for large vessels (> 100 μm diameter) substantially increased when skin preheating was applied

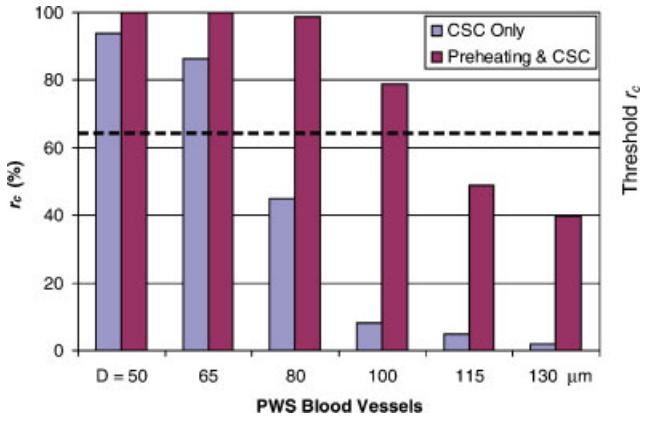

Fig. 7. r_c for vessels of different diameters with CSC only and with both preheating and CSC; MVF = 15%; PWS depth, 200 μm; laser, 3.5 J/cm^2, 1.5 milliseconds.

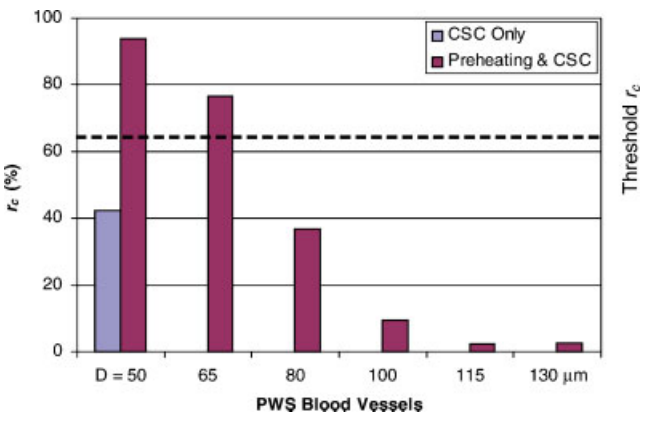

Fig. 8. r_c for vessels of different diameters with CSC only and with both preheating and CSC; MVF = 15%; PWS depth, 400 μm; laser, 3.5 J/cm^2, 1.5 milliseconds.

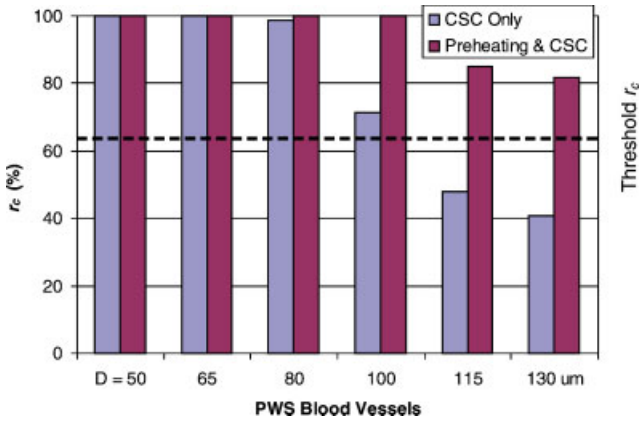

Fig. 9. r_c for vessels of different diameters with CSC only and with both preheating and CSC; MVF = 10%; PWS depth, 400 μm; CSC, 100 milliseconds; laser, 4.5 J/cm^2, 1.5 milliseconds.

prior to CSC. Based on the damage criterion we assumed, diameter of vessels that will be destroyed irreversibly increases from 100 μm for CSC only to 130 μm for both preheating and CSC.

DISCUSSION

Several assumptions were made in the numerical models for this study. The first assumption was that freezing of water has no significant influence on epidermal protection with CSC. In vitro experiments with an epoxy skin phantom indicate that human skin will be exposed to subzero temperatures during CSC and thus possibly be frozen. During the freezing of water in skin, a latent heat of 334 kJ/kg will be released, which is much higher than the sensible heat of skin (~4 kJ/kg for 1°C change). Therefore, the epidermal temperature reduction will be smaller than that measured with the epoxy skin phantom. However, the same amount of latent heat needs to be absorbed during the melting of ice crystals when skin is heated by the laser pulse, which slows down the temperature increase of skin.

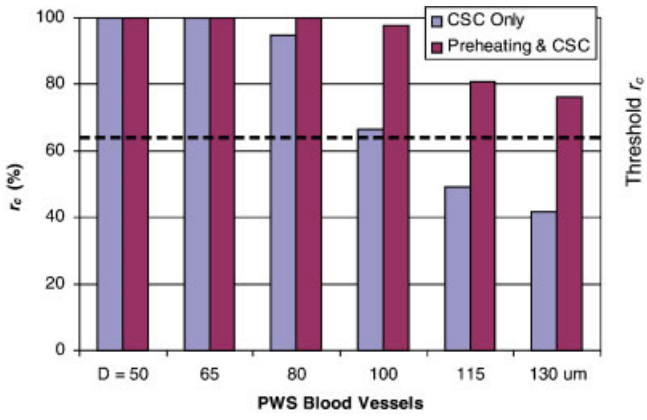

Fig. 10. r_c for vessels of different diameters with CSC only and with both preheating and CSC; MVF = 5%; PWS depth, 900 μm; CSC, 100 milliseconds; laser, 7.0 J/cm^2, 1.5 milliseconds.

Therefore, we assume freezing of water has no significant influence on epidermal protection with CSC.

The second one was that we assume no vaporization/bubble formation occurs, although the numerical results indicate that the simulated blood temperature is 20°C higher than 100°C. The reason is that the bubble nucleation temperature, T_N, should be much higher than 100°C during pulsed laser heating. Both analysis and experiments show that T_N of water increases with heating rate from a few degrees higher than 100°C to the homogeneous vapor bubble nucleation temperature of about 295°C [37,38]. In vitro experiments of open-cuvette pulsed laser irradiation of whole blood has shown that blood temperatures reached 150°C before significant explosive vaporization occurred [35]. The heating rate in that experiment was approximately 13×10^3 °C/second, which is much lower than the heating rate in our simulation of 56×10^3 °C/second. Therefore, T_N in our simulation is even higher than 150°C and our assumption of no vaporization is valid.

The effect of preheating prior to CSC on PWS laser therapeutic outcome depends greatly on blood vessel morphology. Qualitatively, skin preheating will improve the therapeutic outcome in a PWS lesion with large and deep ectatic vessels for all patients regardless of skin type. Quantitative prediction of therapeutic outcome with skin preheating can only be conducted when the criterion to assess irreversible PWS vessel damage is well defined. Therefore, clinical studies on the effect of skin preheating with different methods are urgently required to assess the role of such an approach to the clinical management of patients with PWS.

CONCLUSIONS

CSC experiments at different T_0 with a thin-foil thermocouple cast on an epoxy skin phantom were conducted. The experimental results show that the skin phantom surface can be cooled to similar minimum temperatures regardless of the initial temperatures. Using the experimental CSC heat flux as one boundary condition, laser PWS therapy in conjunction with either CSC or skin preheating prior to CSC was simulated numerically. The results indicate that skin preheating prior to CSC can be effectively used to cool the epidermis to a temperature similar to that expected with CSC alone, and increase blood vessel temperature before laser irradiation. PWS patients may benefit from skin preheating prior to CSC, depending on PWS vessel diameter and depth.

ACKNOWLEDGMENTS

The authors would like to thank Prof. Lars Svaasand and Prof. Sol Kimel for significant discussions regarding this research, Dr. Rong Zhang for discussions regarding the numerical models, and Elaine Kato for proofreading. This work was supported by the National Institutes of Health (GM 62177, AR 48458 and AR 47551 to JSN and HD42057 to GA). Institutional support from the Beckman Laser Institute Endowment is also acknowledged. The CSC methodology described in this manuscript is contained

within U.S. patent no. 5,814,040–Apparatus and Method for Dynamic Cooling of Biological Tissue for Thermal Mediated Surgery, awarded to J. Stuart Nelson, MD, PhD, Thomas E. Milner, PhD, and Lars O. Svaasand, PhD, and assigned to the Regents of the University of California. This work was presented in part at the annual meeting of the American Society for Laser Medicine and Surgery, April 2005, in Orlando, Florida.

REFERENCES

1. Nelson JS, Milner TE, Anvari B, Tanenbaum BS, Kimel S, Svaasand LO, Jacques SL. Dynamic epidermal cooling during pulsed laser treatment of port-wine stain: A new methodology with preliminary clinical evaluation. Arch Dermatol 1995;131(6):695–700.
2. Nelson JS, Milner TE, Anvari B, Tanenbaum BS, Svaasand LO, Kimel S. Dynamic epidermal cooling in conjunction with laser-induced photothermolysis of portwine stain blood vessels. Lasers Surg Med 1996;19(2):224–229.
3. Waldorf HA, Alster TS, McMillan K, Kauvar ANB, Geronemus RG, Nelson JS. Effect of dynamic cooling on 585-nm pulsed dye laser treatment of port-wine stain birthmarks. Dermatol Surg 1997;23(8):657–662.
4. Chang CJ, Nelson JS. Cryogen spray cooling and higher fluence pulsed dye laser treatment improve port-wine stain clearance while minimizing epidermal damage. Dermatol Surg 1999;25(10):767–772.
5. Chang CJ, Kelly KM, Nelson JS. Cryogen spray cooling and pulsed dye laser treatment of cutaneous hemangiomas. Ann Plast Surg 2001;46(6):577–583.
6. Fiskerstrand EJ, Ryggen K, Norvang LT, Svaasand LO. Clinical effects of dynamic cooling during pulsed laser treatment of port-wine stains. Laser Med Sci 1997;12(4): 320–327.
7. Chiu CH, Chan HHL, Ho WS, Yeung CK, Nelson JS. Prospective study of pulsed dye laser in conjunction with cryogen spray cooling for treatment of port wine stains in Chinese patients. Dermatol Surg 2003;29(9):909–915.
8. van der Horst CMAM, Koster PHL, de Borgie CAJM, Bossuyt PMM, van Gemert MJC. Effect of the timing of treatment of port-wine stains with the flash-lamp-pumped pulsed dye-laser. N Engl J Med 1998;338(15):1028–1033.
9. Yohn JJ, Huff JC, Aeling JL, Walsh P, Morelli JG. Lesion size is a factor for determining the rate of port-wine stain clearing following pulsed dye laser treatment in adults. Cutis 1997; 59(5):267–270.
10. Katugampola GA, Lanigan SW. Five years' experience of treating port wine stains with the flashlamp-pumped pulsed dye laser. Br J Dermatol 1997;137(5):750–754.
11. Lanigan SW. Port-wine stains unresponsive to pulsed dye laser: explanations and solutions. Br J Dermatol 1998;139(2): 173–177.
12. Jia WC, Aguilar G, Wang GX, Nelson JS. Heat-transfer dynamics during cryogen spray cooling of substrate at different initial temperatures. Phys Med Biol 2004;49(23): 5295–5308.
13. Sturesson C, Andersson-Engels S. Mathematical modelling of dynamic cooling and pre-heating, used to increase the depth of selective damage to blood vessels in laser treatment of port wine stains. Phys Med Biol 1996;41(3):413–428.
14. Torres JH, Nelson JS, Tanenbaum BS, Milner TE, Goodman DM, Anvari B. Estimation of internal skin temperatures in response to cryogen spray cooling: Implications for laser therapy of port wine stains. IEEE J Sel Top Quant 1999;5(4): 1058–1066.
15. Aguilar G, Wang GX, Nelson JS. Effect of spurt duration on the heat transfer dynamics during cryogen spray cooling. Phys Med Biol 2003;48(14):2169–2181.
16. Svaasand LO, Randeberg LL, Aguilar G, Majaron B, Kimel S, Lavernia EJ, Nelson JS. Cooling efficiency of cryogen spray during laser therapy of skin. Lasers Surg Med 2003;32(2): 137–142.
17. Franco W, Liu J, Wang GX, Nelson JS, Aguilar G. Radial and temporal variations in surface heat transfer during cryogen spray cooling. Phys Med Biol 2005;50(2):387–397.
18. Tunnell JW, Torres JH, Anvari B. Methodology for estimation of time-dependent surface heat flux due to cryogen spray cooling. Ann Biomed Eng 2002;30(1):19–33.
19. Duck FA. Physical properties of tissue: A comprehensive reference book. London, UK: Academic. 1990.
20. Taler J. Theory of transient experimental techniques for surface heat transfer. Int J Heat Mass Transf 1996;39(17): 3733–3748.
21. Keijzer M, Jacques SL, Prahl SA, Welch AJ. Light distributions in artery tissue—Monte-Carlo simulations for finite-diameter laser beams. Lasers Surg Med 1989;9(2):148–154.
22. Keijzer M, Pickering JW, van Gemert MJC. Laser-beam diameter for Port Wine Stain treatment. Lasers Surg Med 1991;11(6):601–605.
23. Lucassen GW, Verkruysse W, Keijzer M, van Gemert MJC. Light distributions in a Port Wine Stain model containing multiple cylindrical and curved blood vessels. Lasers Surg Med 1996;18(4):345–357.
24. Verkruysse W, Lucassen GW, deBoer JF, Smithies DJ, Nelson JS, van Gemert MJC. Modelling light distributions of homogeneous versus discrete absorbers in light irradiated turbid media. Phys Med Biol 1997;42(1):51–65.
25. Verkruysse W, Pickering JW, Beek JF, Keijzer M, van Gemert MJC. Modeling the effect of wavelength on the pulsed dye laser treatment of port wine stains. Appl Optics 1993;32(4):393–398.
26. Jia W, Aguilar G, Nelson JS. Heat transfer dynamics during treatment of port-wine stain birthmarks with multiple-intermittent cryogen spurts and laser pulses. 2005 ASME Summer Heat Transfer Conference; 2005, July 17–22, San Francisco, CA.
27. Martin H. Heat and mass transfer between impinging gas jets and solid surfaces. Adv Heat Transfer 1977;13:1–60.
28. Weaver JA, Stoll AM. Mathematical model of skin exposed to thermal radiation. Aerosp Med 1969;40(1):24–30.
29. Lepock JR, Frey HE, Bayne H, Markus J. Relationship of Hyperthermia-Induced Hemolysis of Human-Erythrocytes to the Thermal-Denaturation of Membrane-Proteins. Biochim Biophys Acta 1989;980(2):191–201.
30. Aguilar G, Wang GX, Nelson JS. Dynamic behavior of cryogen spray cooling: Effects of spurt duration and spray distance. Lasers Surg Med 2003;32(2):152–159.
31. Aguilar G, Majaron B, Karapetian E, Lavernia EJ, Nelson JS. Experimental study of cryogen spray properties for application in dermatologic laser surgery. IEEE Trans Biomed Eng 2003;50(7):863–869.
32. Johnson JM, Brengelmann GL, Hales JRS, Vanhoutte PM, Wenger CB. Regulation of the cutaneous circulation. Fed Proc 1986;45:2841–2850.
33. DeBoer JF, Lucassen GW, Verkruysse W, VanGemert MJC. Thermolysis of port-wine-stain blood vessels: Diameter of a damaged blood vessel depends on the laser pulse length. Lasers Med Sci 1996;11(3):177–180.
34. Pfefer TJ, Barton JK, Smithies DJ, Milner TE, Nelson JS, van Gemert MJC, Welch AJ. Modeling laser treatment of Port Wine Stains with a computer-reconstructed biopsy. Lasers Surg Med 1999;24(2):151–166.
35. Pfefer TJ, Choi B, Vargas G, McNally KM, Welch AJ. Pulsed laser-induced thermal damage in whole blood. J Biomech Eng-T ASME 2000;122(2):196–202.
36. Pickering JW, van Gemert MJC. 585 Nm for the Laser treatment of Port Wine Stains—A possible mechanism. Lasers Surg Med 1991;11(6):616–618.
37. Blander M, Katz JL. Bubble nucleation in liquids. AIChE J 1975;21(5):833–848.
38. Iida Y, Okuyama K, Sakurai K. Boiling nucleation on a very small film heater subjected to extremely rapid heating. Int J Heat Mass Transf 1994;37(17):2771–2780.